Theoretical study of sleeved compression members considering the core protrusion

Chenhui Zhang[a] and Changgen Deng[*]

College of Civil Engineering, Tongji University, Shanghai 200092, China

Abstract. This paper presents a detailed theoretical study of the sleeved compression members based on a mechanical model. In the mechanical model, the core protrusion above sleeve and the contact force between the core and sleeve are specially taken into account. Via the theoretical analyses, load-displacement relationships of the sleeved compression members are obtained and verified by the experimental results. On the basis of the core moment distribution changing with the increase of the applied axial load, failure mechanism of the sleeved compression members is assumed and proved to be consistent with the experimental results in terms of the failure modes and the ultimate bearing capacities. A parametric study is conducted to quantify how essential factors including the core protrusion length above sleeve, stiffness ratio of the core to sleeve, core slenderness ratio and gap between the core and sleeve affect the mechanical behaviors of the sleeved compression members, and it is concluded that the constrained effect of the sleeve is overestimated neglecting the core protrusion; the improvement of ultimate bearing capacity for the sleeved compression member is considered to be decreasing with the decrease of the core slenderness ratio and for the sleeved compression member with core of small slenderness ratio, small gap and small stiffness ratio are preferred to obtain larger ultimate bearing capacity and stiffness.

Keywords: theoretical study; sleeved compression member; load-displacement relationship; failure mechanism; parametric study; buckling constraint

1. Introduction

Due to pursuit of environment friendliness in the structure design and rapid improvement of steel properties towards high strength and light weight, stability of steel structures has become increasingly important, and steel structures are governed to a great extent on stability limit states (Galambos and Surovek 2008). Meanwhile, stability represents a fundamental problem, which must be mastered to ensure the safety of structures against collapse (Bažant 2000). For one thing, local instabilities can terminate service life of the whole structure (Farshad 1994); furthermore, buckling of compression members may lead to progressive collapse (Abedi and Parke 1996) of the structure resulting in catastrophic failures, such as the collapse of the Quebec Bridge (Pearson and Delatte 2006) and the Hartford Civic Center Coliseum (Rachel and Delatte 2001). In view of this, it's of vital importance to constrain member buckling and strengthen the key compression member in the structure.

In the past three decades, different kinds of buckling constrained devices have been developed to strengthen compression members, such as buckling-restrained brace (Inoue *et al.* 2001, Wang *et al.* 2013), prestressed stayed column (Osofero *et al.* 2012) and sleeved compression

member (Sridhara 1993), etc. Only the sleeved compression members, in terms of deadweight and configuration, have the potential to be applied in the spatial grid structures. Therefore, sleeved compression members need to be studied intensively for the potential application in the spatial grid structures to constrain member buckling.

Early researchers Sridhara and Prasad did fundamental work for the sleeved compression members. Sridhara (1993) proposed the idea of sleeved compression members and carried out theoretical and experimental study, making it certain that the sleeved compression members had an improved resistance to buckling. Prasad (1992) excited the core into higher buckling modes and did a parametric study to quantify the effects of different parameters on the behavior of the system. But there were no connections between the core and sleeve with the sleeve positioned depending on the testing facility in their experiments, so their sleeved compression members did not have the feasibility to be applied in the structures.

Recently, Shen (2007), Du (2009), Hu *et al.* (2013) and Shen *et al.* (2016) carried out experimental studies of the improved sleeved compression members in which the core and sleeve were connected at both ends by bolts, polyethylene foam and welding, making it possible for the sleeved compression members to be practically applied. The experimental results showed that the failure of the sleeved compression members was mainly attributed to local buckling near the end of the core. Shen (2007) took into account the contact between the core and sleeve in his theoretical analyses; Hu *et al.* (2013) introduced material nonlinearity into the theoretical analysis and held that the

*Corresponding author, Professor
  E-mail: dengcg@tongji.edu.cn
[a]Ph.D. Student
  E-mail: zhangchenhui0412@163.com

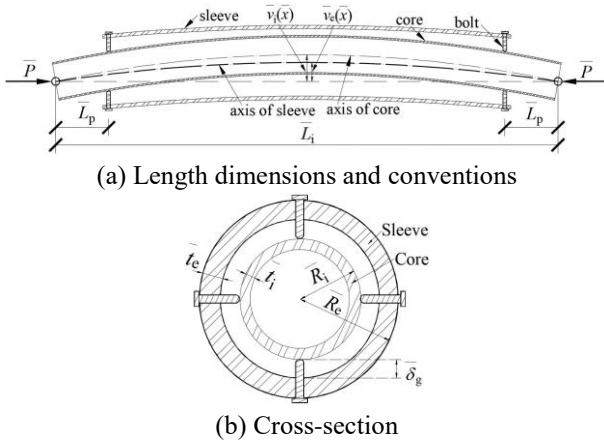(a) Length dimensions and conventions

(b) Cross-section

Fig. 1 Details of the TinT-SCM

system would eventually fail by the yielding of the sleeve, the same opinion of Prasad (1992), which was not true of the improved sleeved compression member and could not reveal the actual failure mechanism. Furthermore, both of them did not consider the core protrusion above sleeve, which might overestimate the constrained effect of the sleeve.

This paper presents a detailed theoretical study of the sleeved compression members on the basis of a mechanical model, taking into account the core protrusion above sleeve. Then the mechanical model is verified by the experimental results in terms of load-displacement relationships. After that, failure mechanism of the sleeved compression members is assumed based on the changing trend of the core moment distribution. And the ultimate bearing capacities of the sleeved compression members are obtained and verified by the experimental results. Last, a parametric study is conducted to quantify the effects of the core protrusion length above sleeve, stiffness ratio of the core to sleeve, core slenderness ratio and gap between the core and sleeve on the mechanical behaviors of the sleeved compression members.

2. Configuration of sleeved compression member

The sleeved compression member referred to as TinT-SCM (Tube-in-Tube Sleeved Compression Member) is composed of an inner tube (core) for load-bearing and an outer tube (sleeve) for buckling-constraining. The two tubes are connected with each other at each end by four bolts proper distance away from the outer tube end, as shown in Fig. 1. The same core protrusion length above sleeve at both ends is to ensure that the core bears the whole axial force and that the TinT-SCM can be connected with other members in the structures. Since the sleeve is positioned by the core via four bolts at each end, there exists translation of the sleeve simultaneous with the core deflection during the deformation process.

For the theoretical study, $\bar{L}_i$ is length of the core; $\bar{A}_i$ is section area of the core; $\bar{E}_i, \bar{E}_e$ are elasticity modulus of the core and sleeve, respectively; $\bar{I}_i, \bar{I}_e$ are inertia moment of the

core and sleeve section, respectively; $\lambda_i = \bar{L}_i / \sqrt{\bar{I}_i / \bar{A}_i}$ is slenderness ratio of the core; $\beta = \bar{E}_i \bar{I}_i / \bar{E}_e \bar{I}_e$ is stiffness ratio of the core to sleeve with $r = \sqrt{\beta/(\beta+1)}$; $\bar{P}_E = \pi^2 \bar{E}_i \bar{I}_i / \bar{L}_i^2$ is Euler buckling load of the core.

The other quantities used are listed with corresponding dimensionless quantities placed behind the commas and nondimensionalized by the equations following closely. Dimensionless quantities are adopted to conduct the theoretical study.

$\bar{x}, x$: parameter in axial direction, $x = \bar{x}/\bar{L}_i$;

$\bar{L}_p, L_p$: core protrusion length above sleeve, $L_p = \bar{L}_p / \bar{L}_i$;

$\bar{\delta}_g, \delta_g$: gap between the core and sleeve, $\delta_g = \bar{\delta}_g / \bar{L}_i$;

$\bar{a}, a$: half the length of line-contact segment, $a = \bar{a}/\bar{L}_i$;

$\bar{P}, p$: axial force applied to the core, $p = \bar{P}/\bar{P}_E$, $\eta = \pi\sqrt{p} = \sqrt{\bar{P}\bar{L}_i^2 / \bar{E}_i \bar{I}_i}$;

$\bar{Q}_0, Q_0$: internal transverse force at bolts, $Q_0 = \bar{Q}_0 \bar{L}_i^2 / \bar{E}_i \bar{I}_i$;

$\bar{F}_0, F_0$: point contact force, $F_0 = \bar{F}_0 \bar{L}_i^2 / \bar{E}_i \bar{I}_i$;

$\bar{q}(\bar{x}), q(x)$: distribution contact force, $q(x) = \bar{q}(\bar{x})\bar{L}_i^3 / \bar{E}_i \bar{I}_i$;

$\bar{M}_i(\bar{x}), M_i(x)$: moment distribution of the core, $M_i(x) = \bar{M}_i(\bar{x})\bar{L}_i / \bar{E}_i \bar{I}_i$;

$\bar{v}_{i0}(\bar{x}), v_{i0}(x)$: initial deflection of the core, $v_{i0}(x) = \bar{v}_{i0}(\bar{x})/\bar{L}_i$;

$\bar{v}_i(\bar{x}), v_i(x)$: total deflection of the core, $v_i(x) = \bar{v}_i(\bar{x})/\bar{L}_i$;

$\bar{v}_e(\bar{x}), v_e(x)$: deflection of the sleeve, $v_e(x) = \bar{v}_e(\bar{x})/\bar{L}_i$;

$\bar{v}, v$: core-center deflection, $\bar{v} = \bar{v}_i(\bar{L}_i/2) - \bar{v}_{i0}(\bar{L}_i/2)$, $v = \bar{v}/\bar{L}_i = v_i(1/2) - v_{i0}(1/2)$;

$\bar{\Delta}, \Delta$: total axial displacement, $\Delta = \bar{\Delta}/\bar{L}_i = \pi^2 p / \lambda_i^2 + \int_0^1 [v_i'(x)]^2 dx/2 - \int_0^1 [v_{i0}'(x)]^2 dx/2$.

3. Theoretical analysis

For the sleeved compression member subjected to increasing axial force *p*, the core deflection grows gradually and point contact occurs between the core and sleeve. Point contact can become line contact as the load increases (Domokos *et al.* 1997). Therefore, three deformation processes are considered including non-contact, point-contact and line-contact process. The contact force between
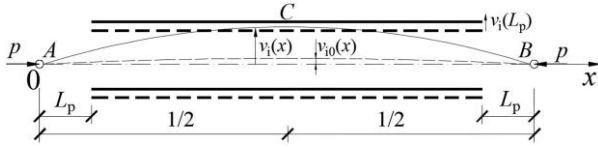
Fig. 2 Displacement process of the core and sleeve before contact

the core and sleeve constrains the core from buckling, and the amplitude and distribution of the contact force determine the constrained effect of the sleeve.

Both the core and sleeve are simplified as beams, and theory of elastic and small deflection is adopted with shear deformation neglected. According to force equilibrium, second-order ordinary differential equations are derived, which can be can be posed as a boundary value problem. In view of standard ODE theory, a unique smooth solution can be obtained depending on the boundary conditions (Robinson 2004).

The following are another four basic assumptions adopted in the theoretical study of the TinT-SCM: (1) the core has an initial geometrical imperfection in the form of $v_{io}(x) = d_0 \sin(\pi x)$ with the amplitude $d_0 = 1/1000$, and the sleeve is perfect; (2) deformation of the core and sleeve is symmetrical about center section; (3) between the core and sleeve at both ends is hinge connections, transferring no axial force and allowing the relative rotation; (4) the friction between the core and sleeve is neglected.

3.1 Non-contact process

The core deflection $v_i(x)$ grows with the increase of axial load p. Meanwhile, translation of the sleeve equal to $v_i(L_p)$ occurs attributed to the connection between the core and the sleeve. There is no deformation in the sleeve and the core is subjected to only the axial force, as shown in Fig. 2.

The equilibrium differential equation of the core is

$$v_i''(x) + \eta^2 v_i(x) = -\pi^2 d_0 \sin(\pi x), \quad (0 \le x \le 1) \tag{1}$$

The boundary conditions of the core are

$$v_i(0) = 0, v_i(1) = 0 \tag{2}$$

The general solution to Eq. (1) is

$$v_i(x) = A\cos(\eta x) + B\sin(\eta x) + \pi^2 d_0 \sin(\pi x)/(\pi^2 - \eta^2), (0 \le x \le 1) \tag{3}$$

Using (2) in Eq. (3), total deflection of the core is

$$v_i(x) = \pi^2 d_0 \sin(\pi x)/(\pi^2 - \eta^2) \tag{4}$$

When $v_i(1/2) - v_i(L_p) = \delta_g$ is true, point contact between the core and sleeve occurs with the axial load $p_N = 1 - d_0 \left[1 - \sin(\pi L_p) \right]/\delta_g$.

3.2 Point-contact process

After the increasing axial force p exceeds p_N, point
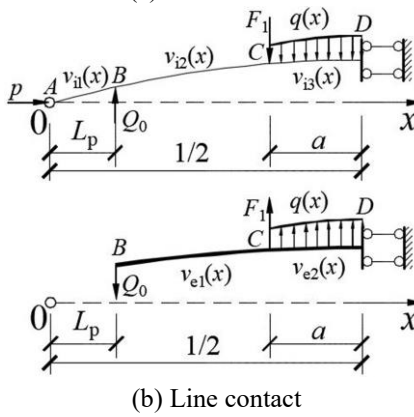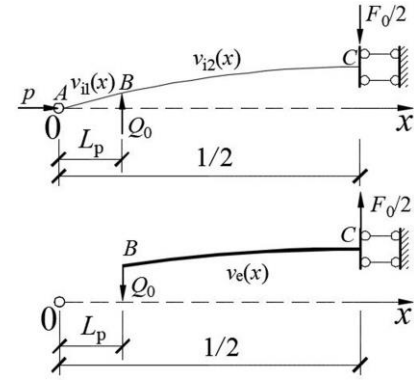

(a) Point contact

(b) Line contact

Fig. 3 Force diagrams of the core and sleeve

contact occurs at point C, center of the core and sleeve. The contact force F_0 is generated at point C with the force Q_0 generated at point B where the bolts are positioned. According to the assumption of the core and sleeve with symmetrical deformation, the half symmetrical TinT-SCM is extracted as shown in Fig. 3(a).

The equilibrium differential equation of the core is

$$\begin{cases} v_{i1}''(x) + \eta^2 v_{i1}(x) = -\pi^2 d_0 \sin(\pi x), (0 \le x \le L_p) \\ v_{i2}''(x) + \eta^2 v_{i2}(x) = -\pi^2 d_0 \sin(\pi x) + Q_0(x - L_p), (L_p \le x \le 1/2) \end{cases} \tag{5}$$

The boundary conditions and the continuity conditions of the core are

$$v_{i1}(0) = 0, \ v_{i2}'(1/2) = 0, v_{i1}(L_p) = v_{i2}(L_p), \ v_{i1}'(L_p) = v_{i2}'(L_p) \tag{6}$$

The general solution to Eq. (5) is

$$\begin{cases} v_{i1}(x) = A_{p1}\cos(\eta x) + B_{p1}\sin(\eta x) + \pi^2 d_0 \sin(\pi x)/(\pi^2 - \eta^2), (0 \le x \le L_p) \\ v_{i2}(x) = A_{p2}\cos(\eta x) + B_{p2}\sin(\eta x) + \pi^2 d_0 \sin(\pi x)/(\pi^2 - \eta^2) + Q_0(x - L_p)/\eta^2, (L_p \le x \le 1/2) \end{cases} \tag{7}$$

Using (6) in Eq. (7), undetermined coefficients in Eq. (7) are obtained with Q_0 unknown.

$$\begin{cases} A_{p1} = 0; B_{p1} = -2Q_0 \sin^2(\eta/4 - L_p\eta/2)/\left[\eta^3 \cos(\eta/2)\right] \\ A_{p2} = Q_0 \sin(L_p\eta)/\eta^3; B_{p2} = Q_0 \left[\sin(L_p\eta)\sin(\eta/2) - 1\right]/\left[\eta^3 \cos(\eta/2)\right] \end{cases} \tag{8}$$

According to the assumption that both ends of the sleeve are hinged, the equilibrium differential equation of the sleeve is

$$v_e''(x) = -\beta Q_0(x - L_p), (L_p \le x \le 1/2) \tag{9}$$

The boundary conditions of the sleeve are

$$v_e\left(L_p\right)=v_{i2}\left(L_p\right),v_e'\left(1/2\right)=0 \qquad (10)$$

The general solution to Eq. (9) is

$$v_e\left(x\right)=-\beta Q_0 x^3/6+\beta Q_0 L_p x^2/2+C_p x+D_p,\left(L_p\leq x\leq 1/2\right) \qquad (11)$$

Using (10) in Eq. (11), undetermined coefficients in Eq. (11) are obtained with Q_0 unknown.

$$\begin{cases}C_p=\left(1-4L_p\right)\beta Q_0/8\\D_p=\dfrac{\pi^2 d_0\sin\left(\pi L_p\right)}{\pi^2-\eta^2}-\dfrac{\left(3L_p-12L_p^2+8L_p^3\right)\beta\eta^3+48\sec(\eta/2)\sin\left(L_p\eta\right)\sin^2\left(\eta/4-L_p\eta/2\right)}{24\eta^3}Q_0\end{cases} \qquad (12)$$

The deformation compatibility condition between the core and sleeve is

$$v_{i2}\left(1/2\right)-v_e\left(1/2\right)=\delta_g+v_{i2}\left(L_p\right) \qquad (13)$$

Using Eq. (13) in Eq. (7) and (11), Q_0 is obtained.

$$Q_0=\dfrac{-24\eta^3\left[\pi^2 d_0+\delta_g\left(\eta^2-\pi^2\right)-2\pi^2 d_0\sin\left(\pi L_p\right)\right]}{\left(\pi^2-\eta^2\right)\left\{\left[\left(1-2L_p\right)^2\beta\eta^2-12\right]\left(2L_p-1\right)\eta+\dfrac{72\sin\left(L_p\eta\right)+24\sin\left(\eta/2-2L_p\eta\right)-48\sin\left(\eta/2\right)}{\cos\left(\eta/2\right)}\right\}} \qquad (14)$$

When $v_{i2}''\left(1/2\right)=v_e''\left(1/2\right)$ is true, point-contact process ends and line-contact process starts with the axial load p_P determined by Eq. (15).

$$A_{p2}\eta^2\cos\left(\eta/2\right)+B_{p2}\eta^2\sin\left(\eta/2\right)+\pi^4 d_0/\left(\pi^2-\eta^2\right)=\beta Q_0\left(1/2-L_p\right) \qquad (15)$$

3.3 Line-contact process

With the increase of p, line contact occurs between the core and sleeve, as shown in Fig. 3(b). There exists internal distribution contact force $q(x)$ in line-contact segment. Concentrated force F_l applied at the end of line-contact segment is to ensure continuous moment of the core and sleeve.

The equilibrium differential equation of the core is

$$\begin{cases}v_{i1}''\left(x\right)+\eta^2 v_{i1}\left(x\right)=-\pi^2 d_0\sin\left(\pi x\right),\left(0\leq x\leq L_p\right)\\v_{i2}''\left(x\right)+\eta^2 v_{i2}\left(x\right)=-\pi^2 d_0\sin\left(\pi x\right)+Q_0\left(x-L_p\right),\left(L_p\leq x\leq 1/2-a\right)\\v_{i3}''\left(x\right)+\eta^2 v_{i3}\left(x\right)=-\pi^2 d_0\sin\left(\pi x\right)+Q_0\left(x-L_p\right)-F_l\left(x-1/2+a\right)-\\\qquad\qquad -\int_{1/2-a}^x q(t)\left(x-t\right)dt,\left(1/2-a\leq x\leq 1/2\right)\end{cases} \qquad (16)$$

The equilibrium differential equation of the sleeve is

$$\begin{cases}v_{e1}''\left(x\right)=-\beta Q_0\left(x-L_p\right),\left(L_p\leq x\leq 1/2-a\right)\\v_{e2}''\left(x\right)=-\beta Q_0\left(x-L_p\right)+\beta F_l\left(x-1/2+a\right)+\beta\int_{1/2-a}^x q(t)\left(x-t\right)dt,\left(1/2-a\leq x\leq 1/2\right)\end{cases} \qquad (17)$$

The deformation compatibility conditions between the core and sleeve are

$$v_{i3}\left(x\right)-v_{e2}\left(x\right)=\delta_g+v_{i1}\left(L_p\right),v_{i3}''\left(x\right)=v_{e2}''\left(x\right),\left(1/2-a\leq x\leq 1/2\right) \qquad (18)$$

Based on that $v_{i3}''\left(x\right)=v_{e2}''\left(x\right)$ is true within the range $\left(1/2-a\leq x\leq 1/2\right)$, integral terms in Eqs. (16)-(17) are eliminated. The general solution to Eq. (16) is

$$\begin{cases}v_{i1}\left(x\right)=A_{L1}\cos\left(\eta x\right)+B_{L1}\sin\left(\eta x\right)+\pi^2 d_0\sin\left(\pi x\right)/\left(\pi^2-\eta^2\right),\left(0\leq x\leq L_p\right)\\v_{i2}\left(x\right)=A_{L2}\cos\left(\eta x\right)+B_{L2}\sin\left(\eta x\right)+\pi^2 d_0\sin\left(\pi x\right)/\left(\pi^2-\eta^2\right)+Q_0\left(x-L_p\right)/\eta^2,\left(L_p\leq x\leq 1/2-a\right)\\v_{i3}\left(x\right)=A_{L3}\cos\left(r\eta x\right)+B_{L3}\sin\left(r\eta x\right)+\pi^2 r^2 d_0\sin\left(\pi x\right)/\left(\pi^2-r^2\eta^2\right),\left(1/2-a\leq x\leq 1/2\right)\end{cases} \qquad (19)$$

and the general solution to Eq. (17) is

$$\begin{cases}v_{e1}\left(x\right)=-\beta Q_0 x^3/6+\beta Q_0 L_p x^2/2+C_L x+D_L,\left(L_p\leq x\leq 1/2-a\right)\\v_{e2}\left(x\right)=A_{L3}\cos\left(r\eta x\right)+B_{L3}\sin\left(r\eta x\right)+\pi^2 r^2 d_0\sin\left(\pi x\right)/\left(\pi^2-r^2\eta^2\right)-\\\qquad\qquad -B_{L1}\sin\left(\eta L_p\right)-\pi^2 d_0\sin\left(\pi L_p\right)/\left(\pi^2-\eta^2\right)-\delta_g,\left(1/2-a\leq x\leq 1/2\right)\end{cases} \qquad (20)$$

The boundary conditions and the continuity conditions of the core are

$$\begin{cases}v_{i1}\left(0\right)=0,\ v_{i3}'\left(1/2\right)=0,v_{i1}\left(L_p\right)=v_{i2}\left(L_p\right)\\v_{i2}\left(1/2-a\right)=v_{i3}\left(1/2-a\right),v_{i1}'\left(L_p\right)=v_{i2}'\left(L_p\right),v_{i2}'\left(1/2-a\right)=v_{i3}'\left(1/2-a\right)\end{cases} \qquad (21)$$

The boundary conditions and the continuity conditions of the sleeve are

$$v_{e1}\left(L_p\right)=v_{i1}\left(L_p\right),v_{e2}'\left(1/2\right)=0,v_{e1}\left(1/2-a\right)=v_{e2}\left(1/2-a\right),v_{e1}'\left(1/2-a\right)=v_{e2}'\left(1/2-a\right) \qquad (22)$$

The condition to ensure continuous moment of the core and sleeve at the section $x=1/2-a$ is

$$v_{e2}''\left(1/2-a\right)=v_{i3}''\left(1/2-a\right)=-\beta Q_0\left(1/2-a-L_p\right) \qquad (23)$$

Using (18), (21), (22) and Eq. (23) in Eqs. (19)-(20), undetermined coefficients A_{L1}, A_{L2} A_{L3}, B_{L1}, B_{L2}, B_{L3}, C_L, D_L and Q_0 are obtained and not explicitly presented due to space limitations. The theoretical results of line-contact process are presented in the following load-displacement relationships.

In the line-contact process, the length of line-contact segment is related to the axial load p with the relationship shown in Eq. (24), from which a can be obtained if the axial load p is given.

$$\begin{aligned}&-A_{L2}\eta\sin\left(\eta/2-\eta a\right)+B_{L2}\eta\cos\left(\eta/2-\eta a\right)+\pi^3 d_0\cos\left(\pi/2-\pi a\right)/\left(\pi^2-\eta^2\right)+Q_0/\eta^2=\\&=-A_{L3}r\eta\sin\left(r\eta/2-r\eta a\right)+B_{L3}r\eta\cos\left(r\eta/2-r\eta a\right)+\pi^3 r^2 d_0\cos\left(\pi/2-\pi a\right)/\left(\pi^2-r^2\eta^2\right)\end{aligned} \qquad (24)$$

When the line-contact segment buckles as a Euler column having clamped ends (Chai 1998), the line-contact process ends with the axial force $p_L=1/a^2$. The corresponding p_L and a can be obtained combining Eq. (24); meanwhile, deflections of the core and sleeve are also considered to determine the end of the line-contact process.

4. Experimental and theoretical analysis results

The mechanical behaviors of the TinT-SCMs were experimentally studied by Shen (2007), and the results are presented briefly as follows.

4.1 Specimens

Three specimens were designed and tested in the experiment. For the TinT-SCMs illustrated in Fig. 1, the core and sleeve were fabricated from seamless Q235 steel circular tubes. According to the results of material tests, a simplified elasto-plastic constitutive model was adopted with $\bar{E}_i=\bar{E}_e=2.06\times10^5\,\mathrm{MPa}$ and yielding stress of the core and sleeve $\bar{f}_y=280.1\mathrm{MPa}$. The detailed geometrical

Table 1 Basic parameters of the specimens

Specimen no.	$\bar{L}_1$/mm	$\bar{L}_p$/mm	$\bar{R}_i$/mm	$\bar{t}_i$/mm	$\bar{R}_e$/mm	$\bar{t}_e$/mm	$\bar{\delta}_g$/mm	$\bar{P}_E$/kN
E1A	2098	158.5	22.5	4	51	14	14.5	50.48
E2A	2098	158	22.5	4	47.5	5	20	50.48
E3A	2440	150	22.5	4	47.5	8	17	37.32

(a) One-way blade hinge supports

(b) Sliding hinge

(c) Fixed hinge

Fig. 4 Connections

parameters were listed in Table 1.

4.2 Experimental facilities

A static loading test was conducted to study the mechanical behaviors of the TinT-SCMs. The one-way blade hinge supports illustrated in Fig. 4(a), where the axial load was applied gradually, were connected to both ends of the core to approximately achieve hinge connection. Two types of connections between the core and sleeve were employed: four round head bolts shown in Fig. 4(b) at one end to approximately achieve sliding hinge connection and four flat head bolts shown in Fig. 4(c) at the other end to approximately achieve fixed hinge connection.

Strain gauges were used to measure the strain of certain core sections and displacement meters were used to measure the core axial displacement and core-center deflection.
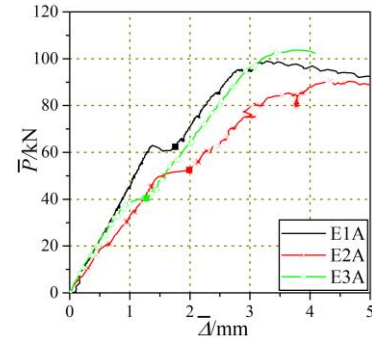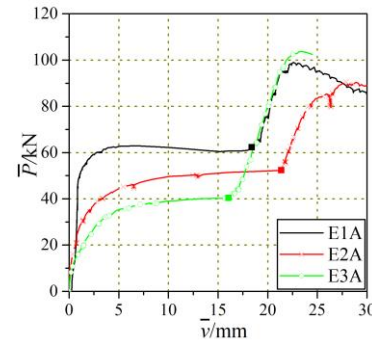

(a) $\bar{P}$ versus $\bar{\Delta}$ curves

(b) $\bar{P}$ versus $\bar{v}$ curves
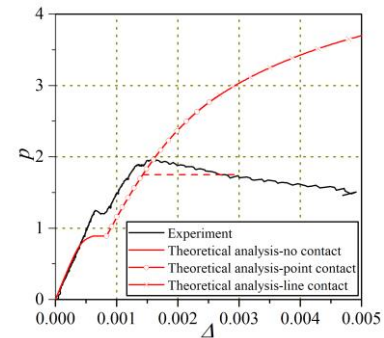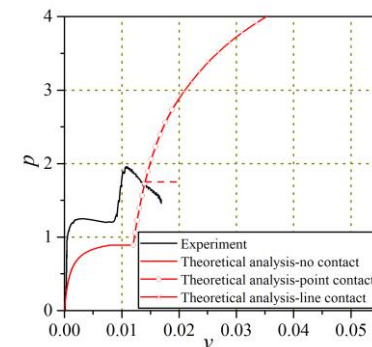
Fig. 5 Experimental results

(a) p versus Δ curves

(b) p versus v curves

Fig. 6 Theoretical analysis result of E1A

4.3 Experimental results

The experimental results are illustrated in Fig. 5 including the axial load versus axial displacement relationships and axial load versus core-center deflection
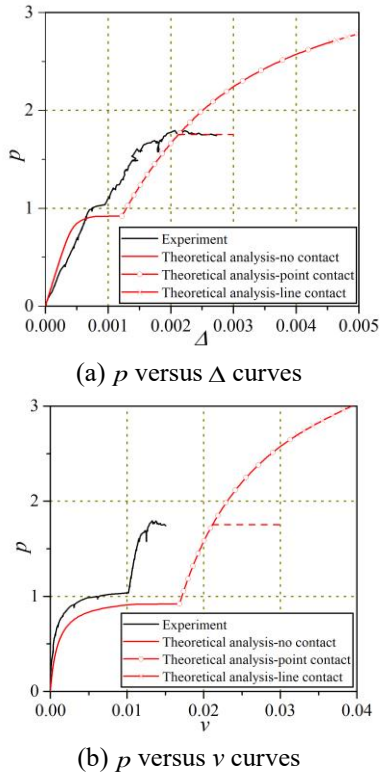
(a) *p* versus Δ curves

(b) *p* versus *v* curves

Fig. 7 Theoretical analysis result of E2A

(a) *p* versus Δ curves

(b) *p* versus *v* curves

Fig. 8 Theoretical analysis result of E3A

relationships. The solid square of same color with the curve stands for point contact occurring between the core and sleeve.

As shown in Fig. 5, the bearing capacities of the TinT-SCMs increase attributed to point contact by 117.8% on average comparing with $\overline{P}_E$, so the TinT-SCMs have an improved resistance to buckling and can be used to constrain member buckling. Furthermore, considering geometrical dimensions of the specimens, the results of E1A and E2A are not as accurate as that of E3A for there exists deviation of E2A with smaller initial stiffness and of E1A with larger axial load at which point contact occurs.

4.4 Theoretical analysis results

Via theoretical analyses, the *p* versus Δ curves and *p* versus *v* curves of the three specimens are illustrated in Figs. 6-8.

As shown in Figs. 6-8, the load-displacement relationships of the three specimens obtained from theoretical analyses are consistent with that from the experiment in terms of the curve development trend. But the loads at which point contact occurs in the experiment are larger than that in the theoretical analyses and $\overline{P}_E$. In addition, the stiffnesses of the TinT-SCMs obtained from theoretical analyses are smaller than that from the experiment. Therefore, relative rotation between the core and sleeve is considered to be limited to some extent by the actual bolt connection which is simplified as hinge connection in the theoretical analysis. Limited relative rotation between the core and sleeve has a positive effect on
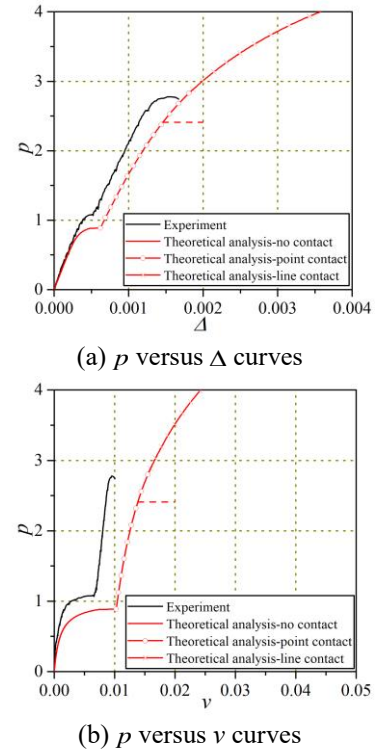
the bearing capacity and stiffness of the TinT-SCM, so the simplification of the actual connection as hinge connection is conservative resulting in larger axial displacement and core-center deflection of the TinT-SCM subjected to the same axial load.

4.5 Failure mechanism

The section plasticity modulus of the core is $\overline{W}_p = 4\overline{R}_i^3/3 - 4(\overline{R}_i - \overline{t}_i)^3/3$. The full-section plastic moment is $\overline{M}_p = \overline{W}_p \overline{f}_y$ and the full-section plastic moment affected by the axial force $\overline{P}$ is $\overline{M}_{pc} = \overline{M}_p \cos\left[\pi\overline{P}/(2\overline{P}_y)\right]$ with $\overline{P}_y = 2\pi(\overline{R}_i - \overline{t}_i/2)\overline{t}_i\overline{f}_y$. The internal forces of core section include the axial force and moment, so the edge stress of core section is $\overline{\sigma}(\overline{x}) = \overline{P}/\overline{A}_i + \overline{M}_i(\overline{x})\overline{R}_i/\overline{I}_i$ with $\overline{M}_i(\overline{x}) = M_i(x)\overline{E}_i\overline{I}_i/\overline{L}_i = \left[-v_i''(x) + v_{i0}''(x)\right]\overline{E}_i\overline{I}_i/\overline{L}_i$ and $\overline{P} = p\overline{P}_E = p\pi^2\overline{E}_i\overline{I}_i/\overline{L}_i^2$.

Failure mechanism of the TinT-SCMs is studied, taking specimen E3A as an example. In the non-contact process, the core moment at section *C* (Fig. 2) is maximum. At the end of this process, the maximum edge stress of section *C* is equal to 206.9 Mpa, smaller than the yielding stress $\overline{f}_y$. In the point-contact process, the core section with maximum moment shifts gradually to the core end, as shown in Fig. 9(a). Attributed to the contact force, the section with maximum moment changes from section *x*=0.5 to section *x*=0.227 with the axial force changing from $0.884\overline{P}_E$ to
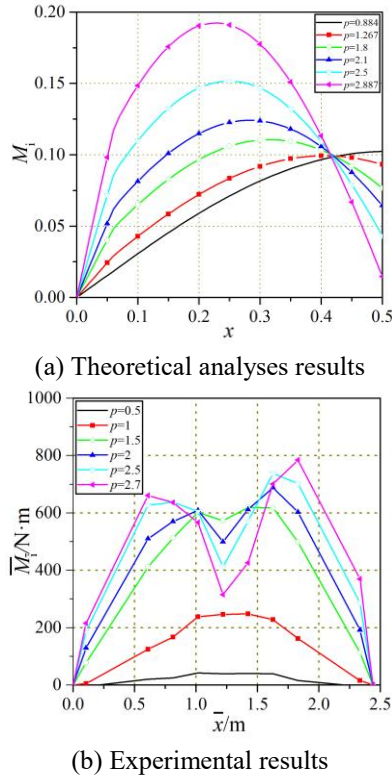
(a) Theoretical analyses results

(b) Experimental results

Fig. 9 Changing trend of the core moment distribution

(a) E1A

(b) E3A

Fig. 10 Failure modes of the specimens

(a) p versus Δ curve of E1A

(b) p versus Δ curve of E3A

Fig. 11 Effect of the core protrusion length

$2.887\bar{P}_E$. The maximum core moment increases unlimitedly neglecting the plasticity. When the axial force reaches $p=1.267$, the edge stress of section $x=0.405$ is equal to the yielding stress $\bar{f}_y$, and the core moment of section $x=0.405$ is defined as $\bar{M}_y$. As shown in Fig. 9(b), the changing trend of core section with maximum moment is verified by the experiment results calculated on the basis of the strain measured. As stated above, larger deflection of the core is obtained from the theoretical analysis. Furthermore, plasticity cannot be considered in the deformation process of the core. Therefore, there exists difference between the core moment in Fig. 9(a) and that in Fig. 9(b) with the core moment in Fig. 9(a) larger.

Attributed to the plasticity development, the core moment increases exceeding $\bar{M}_y$ and the core moment should be limited. As the plasticity development coefficient of circular tube is 1.15 (GB50017 2017), an assumption is made that the ultimate section moment is equal to $1.15\bar{M}_y$ during the deformation process of $p>1.267$. The full-section plastic moment $\bar{M}_{pc}$ of the core decreases with the increase of axial load p. Once $\bar{M}_{pc}=1.15\bar{M}_y$ is satisfied, the TinT-SCM is considered to fail attributed to local buckling occurring near the core end. The failure modes of the specimens in the experiment are illustrated in Fig. 10, which is also attributed to local buckling near the core ends and consistent with the failure mechanism assumed. The ult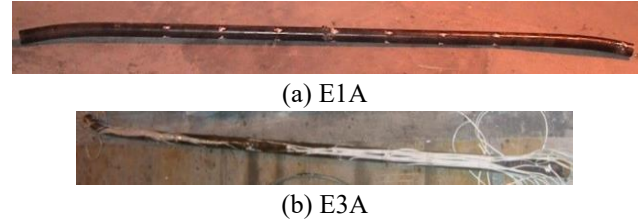imate bearing capacities of the three specimens are illustrated by dashed lines in Figs. 6-8 with acceptable differences from the experimental results.
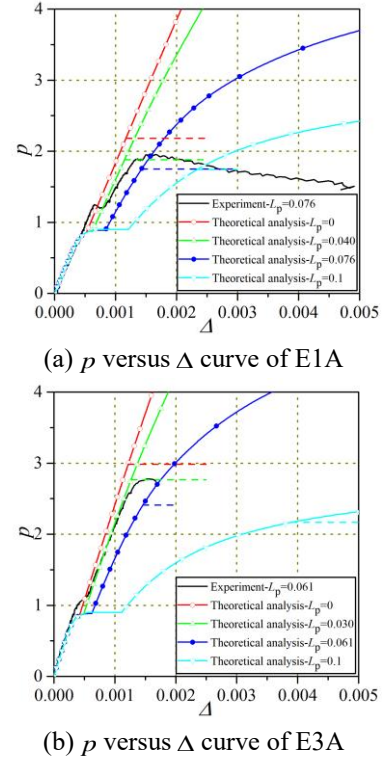
It is concluded that affected by the contact force, the section with maximum moment is closer to the core ends with the increase of axial load, and local buckling of the core occurs if the ultimate moment $1.15\bar{M}_y$ is equal to the full-section plastic moment $\bar{M}_{pc}$, which supplies theoretical basis for strengthening the core. Load-displacement relationships obtained from theoretical analyses are consistent with that from the experiment. Therefore, the theoretical model can be used for preliminary design of the TinT-SCM. But global buckling of the TinT-SCMs, which possibly but rarely occurs, cannot be considered based on the theoretical model.

5. Parametric study

Parametric studies are conducted to qualify the effects of essential factors on the ultimate bearing capacities and the stiffnesses of the TinT-SCMs. The parametric studies center on four factors: core protrusion length above sleeve,
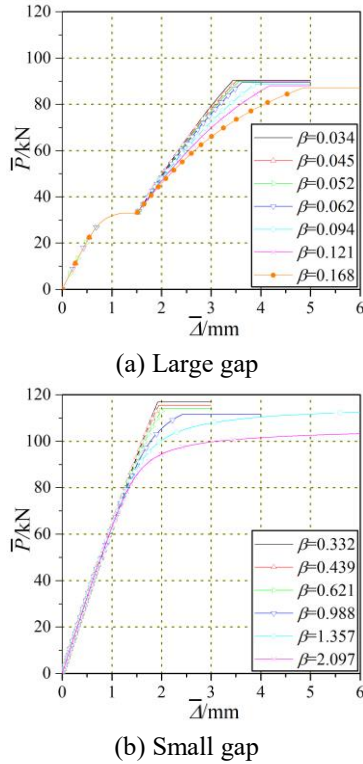
(a) Large gap

(a) Small gap

(b) Small gap

Fig. 12 Effect of stiffness ratio of the core to sleeve

(b) Large gap

Fig. 13 Effect of core slenderness ratio

stiffness ratio of the core to sleeve, core slenderness ratio and gap between the core and sleeve.

5.1 Effect of the core protrusion length above sleeve

The core protrusion lengths above sleeve are changed with the other dimensions equal to that of specimens E1A and E3A. The p versus Δ curves are illustrated in Fig. 11.

It is concluded that the analysis result of the specimen with the actual core protrusion considered is more consistent with the experimental result in terms of the curve development trend. The specimen analyzed neglecting the core protrusion has larger bearing capacity and stiffness overestimating constrained effect of the sleeve. Furthermore, the bearing capacity and stiffness are rapidly decreasing with the increase of protrusion length. Therefore, the core protrusion above sleeve should be controlled in the design of the TinT-SCM.

5.2 Effect of the stiffness ratio

Due to the configuration of the TinT-SCM, the stiffness ratio of the core to sleeve decreases inevitably with the increase of the gap between the core and sleeve. The effect of stiffness ratio of the core to sleeve is studied in two cases only changing the sleeve thickness: (1) large-gap TinT-SCMs with sleeve sections $\phi85\times3$, $\phi87\times4$, $\phi89\times5$, $\phi93\times7$, $\phi97\times9$, $\phi101\times11$ (2) small-gap TinT-SCMs with sleeve sections $\phi52\times1$, $\phi53\times1.5$, $\phi54\times2$, $\phi56\times3$, $\phi58\times4$, $\phi60\times5$. The core section is $\phi45\times4$, the core length $\overline{L}_i$ is 2440 mm and the core protrusion length $\overline{L}_p$ is 150 mm. It is assumed
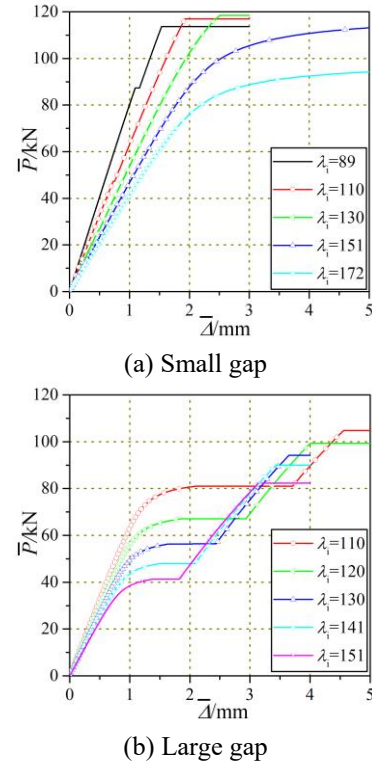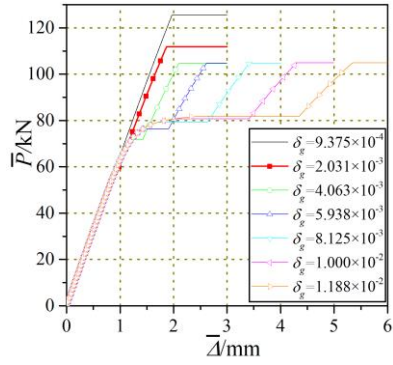
that no failure of the sleeve occurs. $\overline{P}$ versus $\overline{\Delta}$ curves are illustrated in Fig. 12.

As shown in Fig. 12, for the TinT-SCM with large gap, the stiffness ratio has an effect on the stiffness but has almost no effect on the ultimate bearing capacity; for the TinT-SCM with small gap, thicker sleeve (small stiffness ratio) is preferred to obtain larger ultimate bearing capacity. In general, the stiffness ratio is almost guaranteed due to the configuration of the TinT-SCM as long as no local failure of the sleeve occurs.
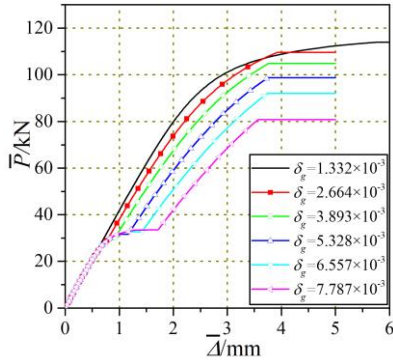
5.3 Effect of core slenderness ratio

The effect of core slenderness ratio is studied in two cases: (1) small-gap TinT-SCMs with the core and sleeve sections $\phi45\times4$ and $\phi60\times5$ (2) large-gap TinT-SCMs with the core and sleeve sections $\phi45\times4$ and $\phi95\times8$. The core protrusion length $\overline{L}_p$ is 150 mm. $\overline{P}$ versus $\overline{\Delta}$ curves are illustrated in Fig. 13.

It is observed that the TinT-SCM with core of small slenderness ratio has larger ultimate bearing capacity but the effect of core slenderness ratio is affected by the gap between the core and sleeve. The core slenderness ratio within certain range has almost no effect on ultimate bearing capacity of the TinT-SCM with small gap, but the ultimate bearing capacity increases with the decrease of core slenderness ratio for the TinT-SCM with large gap. In addition, the improvement (elevation ratio against $\overline{P}_E$) of ultimate bearing capacity is considered to be decreasing with the decrease of core slenderness ratio for the TinT-SCM.

(a) Small core slenderness ratio

(b) Large core slenderness ratio

Fig. 14 Effect of gap between the core and sleeve
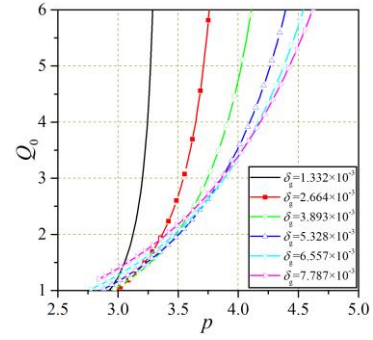
5.4 Effect of the gap

The effect of gap is studied in two cases with the same sleeve thickness: (1) TinT-SCMs of small core slenderness ratios with $\bar{L}_1$=1600mm and sleeve sections ϕ60×6, ϕ63.5×6, ϕ70×6, ϕ76×6, ϕ83×6, ϕ89×6, ϕ95×6 (2) TinT-SCMs of large core slenderness ratios with $\bar{L}_1$=2440mm and sleeve sections ϕ63.5×6, ϕ70×6, ϕ76×6, ϕ83×6, ϕ89×6, ϕ95×6. The core section is ϕ45×4 and the core protrusion length $\bar{L}_p$ is 150 mm. $\bar{P}$ versus $\bar{\Delta}$ curves are illustrated in Fig. 14.

It is observed that the TinT-SCM with small gap has larger ultimate bearing capacity and stiffness but the effect of gap is affected by the core slenderness ratio. The gap within certain range has almost no effect on the ultimate bearing capacity of the TinT-SCM with core of small slenderness ratio, but the ultimate bearing capacity and stiffness increase with the decrease of the gap for the TinT-SCM with core of large slenderness ratio.

It is concluded that there exist mutual effects between the gap and the core slenderness ratio. For the TinT-SCM with core of small slenderness ratio, smaller gap and small stiffness ratio are preferred to obtain larger ultimate bearing capacity and stiffness.

5.5 Effect of the gap on contact force

To study the effect of the gap on the contact force Q_0, the sleeve sections vary among ϕ63.5×6, ϕ70×6, ϕ76×6, ϕ83×6, ϕ89×6, ϕ95×6 with other dimensions equal to that of

Fig. 15 The Q_0 versus p curves

specimen E3A.

When the core segments near the two ends are strengthened, line contact is estimated to occur with the increase of axial load p. The Q_0 versus p curves in the line-contact process are illustrated in Fig. 15 revealing that the contact force increases rapidly with the decrease of the gap between the core and sleeve. The rapidly increasing contact force may generate excessive friction force between the core and sleeve.

The TinT-SCM with smaller gap has larger bearing capacity, but excessive friction forces between the core and sleeve may be generated. It's of vital importance to balance the bearing capacity and the friction force between the core and sleeve considering the hysteretic behavior of the TinT-SCM. Excessive friction force and subsequent unbalanced tension and compression characteristic of the TinT-SCM may result in unexpected design problem.

6. Conclusions

In this paper, a mechanical model is established for the TinT-SCM with the core protrusion above sleeve and the contact force between the core and sleeve taken into account. The mechanical model is verified by the experimental results in terms of load-displacement relationships. Based on the changing trend of the core moment distribution with the increase of the applied axial load, the failure mechanism of the TinT-SCMs is assumed and verified by the experimental results in terms of the failure modes and the ultimate bearing capacities. Finally, the effects of essential factors on the mechanical behaviors of the TinT-SCMs are quantified. Several conclusions are as follows:

• In view of the consistency of load-displacement relationships obtained from the theoretical analyses and experimental study of the TinT-SCMs, the established mechanical model can be used for preliminary design of the TinT-SCMs.

• The contact force affects the position of the core section with maximum moment. With the increase of the axial load, the core section with maximum moment shifts gradually to the core end resulting in local buckling of the core near the end.

• The core protrusion above sleeve has an effect on the mechanical behavior of the TinT-SCM and the constrained

effect of the sleeve is overestimated neglecting the core protrusion.

• Stiffness ratio of the core to sleeve, core slenderness ratio and gap between the core and sleeve affect the mechanical behaviors of the TinT-SCMs. The improvement of ultimate bearing capacity for the TinT-SCM is considered to be decreasing with the decrease of core slenderness ratio. Small gap and small stiffness ratio are preferred for the TinT-SCM with core of small slenderness ratio to obtain large ultimate bearing capacity and stiffness.

Acknowledgments

References

Abedi, K. and Parke, G.A.R. (1996), "Progressive collapse of single-layer braced domes", *Int. J. Space Struct.*, **11**(3), 291-306.

Bažant, Z.P. (2000), "Structural stability", *Int. J. Sol. Struct.*, **37**, 55-67.

Chai, H. (1998), "The post-buckling response of a bi-laterally constrained column", *J. Mech. Phys. Sol.*, **46**(7), 1155-1181.

Domokos, G., Holmes, P. and Royce, B. (1997), "Constrained Euler buckling", *J. Nonlin. Sci.*, **7**(3), 281-314.

Du, Y. (2009), "Seismic performance of the sleeved column of buckling-restrained brace", M.Sc. Dissertation, Inner Mongolia University of Science and Technology, Baotou, China.

Farshad, M. (1994), *Stability of Structures*, Elsevier, Amsterdam, the Netherlands.

Galambos, T.V. and Surovek, A.E. (2008), *Structural Stability of Steel: Concepts and Applications for Structural Engineers*, John Wiley & Sons, Inc., New Jersey, U.S.A.

GB50017 (2017), *Code for Design of Steel Structures*, Ministry of Housing and Urban-Rural Development of the People's Republic of China, Beijing, China.

Hu, B., Gao, B.Q., Zhan, S.L. and Zhang, C. (2013), "Theoretical and experimental study on load-carrying capacity of combined members consisted of inner and sleeved tubes", *Struct. Eng. Mech.*, **45**(1), 129-144.

Inoue, K., Sawaizumi, S. and Higashibata, Y. (2001), "Stiffening requirements for unbonded braces encased in concrete panels", *J. Struct. Eng.*, **127**(6), 712-719.

Osofero, A.I., Wadee, M.A. and Gardner, L. (2012), "Experimental study of critical and post-buckling behavior of prestressed stayed columns", *J. Constr. Steel Res.*, **79**, 226-241.

Pearson, C. and Delatte, N. (2006), "Collapse of the Quebec Bridge, 1907", *J. Perform. Constr. Fac.*, **20**(1), 84-91.

Prasad, B.K. (1992), "Experimental investigation of sleeved column", *Proceedings of the 33rd Structures, Structural Dynamics and Materials Conference*, Dallas, April.

Rachel, M. and Delatte, N.J. (2001), "Another look at Hartford civic center coliseum collapse", *J. Perform. Constr. Fac.*, **15**(1), 31-36.

Robinson, J.C. (2004), *An Introduction to Ordinary Differential Equations*, Cambridge University Press, Cambridge, U.K.

Shen, B. (2007), "Theoretical and experimental investigations on the static stability of sleeved compression members", Ph.D. Dissertation, Tongji University, Shanghai, China.

Shen, J., Seker, O., Sutchiewcharn, N. and Akbas, B. (2016),

"Cyclic behavior of buckling-controlled braces", *J. Constr. Steel Res.*, **121**, 110-125.

Sridhara, B.N. (1993), *Sleeved Compression Member*, U.S. Patent and Trademark Office, Washington, U.S.A.

Wang, C.L., Usami, T., Funayama, J. and Imase, F. (2013), "Low-cycle fatigue testing of extruded aluminum alloy buckling-restrained braces", *Eng. Struct.*, **46**, 294-301.

CC